Chapter 5
The Quartz Crystal Microbalance as a Nanotribology Technique

Lorenzo Bruschi and Giampaolo Mistura

Abstract The quartz crystal microbalance (QCM) technique is a powerful probe of interfacial phenomena that has been successfully employed to investigate the sliding friction of objects of nanoscopic size subject to lateral speeds as large as a few m/s. After a description of the quartz acoustics, the chapter presents the more common circuits used to drive the QCM and discusses the main problems in the application of such a technique to the study of nanotribolgoy; the quality of the surface electrodes and surface contamination.

5.1 Introduction

The quartz crystal microbalance (QCM) technique is a powerful probe of interfacial phenomena that has been successfully employed to investigate the sliding friction of objects of nanoscopic size subject to lateral speeds as large as a few m/s [1, 2]. The microbalance is a small quartz disk whose principal faces are optically polished and covered by two metal films, which are used both as electrodes and as adsorption surfaces. By applying an AC voltage across the two electrodes, it is possible to drive the crystal to its own mechanical resonance with the two parallel faces oscillating in a transverse shear motion. The quality factor of these resonances is usually very high ($\gtrsim 10^5$) and this explains why the QCM is quite sensitive to interfacial phenomena. A change in the disk inertia, as caused, for example, by the adsorption of a film on the metal electrodes, is signalled by a shift in the resonant frequency. Similarly, any dissipation taking place in the system determines a decrease in the resonance amplitude.

L. Bruschi (✉)
CNISM Unitá di Padova, via Marzolo 8, 35131 Padova, Italy
e-mail: lorenzo.bruschi@unipd.it

G. Mistura
CNISM and Dipartimento di Fisica e Astronomia G. Galilei, Universitá di Padova, via Marzolo 8, 35131 Padova, Italy
e-mail: giampaolo.mistura@unipd.it

E. Gnecco and E. Meyer (eds.), *Fundamentals of Friction and Wear on the Nanoscale*, NanoScience and Technology, DOI 10.1007/978-3-319-10560-4_5

Thanks to the pioneer work of Krim and coworkers [3], it was found that molecules and atoms weakly bound to the surface of a quartz crystal can slip relative to the oscillating substrate. The slip occurs as a result of the force of inertia F acting on the adsorbates during the vibrational motion of the crystal. Actually, because of its extremely small value, the force F induces a slow, thermally activated motion of the adsorbate along its direction, with a drift velocity proportional to F. Most of the friction experiments carried out so far with the QCM technique have dealt with molecularly thin films of simple gases adsorbed at low temperatures on the metal electrodes, generally gold or silver, evaporated over the faces of a quartz crystal. For such studies, the QCM was implemented in standard cryostats that guarantee very good temperature controls, of the order of a few mK or better [4–7]. In this way, it was possible to achieve very stable quartz resonance curves, an essential requirement to detect the tiny dissipation associated with the friction of very thin films. However, more systematic and quantitative investigations now require the use of very uniform and clean surfaces, well characterized at the microscopic level by techniques like STM or AFM. Furthermore, it is also important to change in-situ and in a controlled way the morphology of the surface. In other words, it is necessary to design a new generation of QCM experiments that combine cryogenics with surface science [8].

In the literature, there are several general reviews on the application of the QCM to nanotribology. However, none of them has covered in detail the experimental aspects of such a technique. Therefore, in this chapter, after a brief description of the acoustics of the QCM, we present the main electronic circuits used to drive the QCM, emphasizing their pro and con. We then discuss the surface quality of the quartz electrodes and conclude with a short summary of the main features of a new apparatus that we have expressly built to fulfil the requirements of low temperatures and an ultra-high-vacuum environment. Finally, we present some preliminary data acquired with set-up that seem to suggest structural depinning of Ne films adsorbed on Pb(111) at a coverage above 0.4–0.5 layers.

5.2 The Acoustics of Quartz Crystal

The more common quartz crystals used in interfacial physics are of the so called AT-cut. It has been extensively used in the electronics because the temperature dependence of its resonance frequency is very small around room temperature. Other types are the SC-cut (stress-compensated) quartz crystal, which is insensitive to radial stresses, although the minimum of the quartz resonance versus temperature curve occurs close to 200 °C. Furthermore, the SC-cut crystals are much more expensive and require a complicated driving circuit with respect to the more common AT-cut crystals. In practice, QCMs employing SC-cut crystals have been used so far in adsorption studies but not in the field of nanotribology [9].

Let us now consider an AT-cut quartz plate, which is characterized by a shear motion of its two parallel faces. The AT crystal has a natural mechanical resonance when the plate thickness h is half of the transverse mode wavelength λ, or an odd

multiple of $\lambda/2$, e.g. $h = n\frac{\lambda}{2}$, where n is called the overtone number ($n = 1$ is the fundamental mode, $n = 3$ is the third overtone…). At room temperature, the resonance frequency of such a plate oscillating in vacuum is related to its thickness h by the simple relation:

$$f_{0,n} = \frac{1.75n}{h} - C \tag{5.1}$$

where $f_{0,n}$ is measured in MHz, h in mm and C is a small correction factor which increases with electrode thickness [10] . (Typical values of $f_{0,1}$ for AT plates employed as QCM sensors lie in the range 1–10 MHz).

At a certain frequency f*, its behavior in vacuum can be described by a complex acoustical impedance:

$$Z_0 \equiv R_0 - jX_0 = R_0 - j\pi\, n\, A\, Z_q \frac{f^* - f_{0,n}}{f_{0,n}} \tag{5.2}$$

where A is the area of one electrode, $Z_q = 8.862 \times 10^5 g/cm^2$ sec is the quartz acoustic impedance and the dissipative term R_0, which accounts for all the losses in the plate, is related to the quality factor Q_0 via

$$\frac{1}{Q_0} = \frac{2R_0}{\pi\, n\, A\, Z_q} \tag{5.3}$$

When the quartz plate is immersed in a fluid, its impedance will change because of the adsorption of a film onto the quartz surfaces and of the viscous coupling with the surrounding vapor. The global contribution per unit area can be expressed in terms of a complex impedance $R_{sfv} - jX_{sfv}$, in series with Z_0. If both faces of the quartz plate are exposed to the fluid, the total dissipative and inertial terms become, respectively, $R_0 + 2AR_{sfv}$ and $X_0 + 2AX_{sfv}$. The quality factor will then decrease by an amount $\Delta\frac{1}{Q}$ equal to:

$$\Delta\frac{1}{Q} \equiv \frac{1}{Q} - \frac{1}{Q_0} = \frac{4R_{sfv}}{\pi\, n\, Z_q} \tag{5.4}$$

and the resonance frequency f will also be diminished by:

$$\Delta f \equiv f - f_{0,n} = -2X_{sfv}\frac{f_{0,n}}{\pi\, n\, Z_q} \tag{5.5}$$

The exact shifts will obviously depend on the explicit forms of R_{sfv} and X_{sfv}. In order to determine them, we have applied the linearized Navier–Stokes equation to the combined system quartz crystal-adsorbed film-bulk vapor [11]. Let d be the thickness of the adsorbed film and ρ_f and η_f its bulk mass density and viscosity, respectively, while η_v and ρ_v represent the viscosity and the density of the bulk vapor. If we assume, as customary, that the transverse velocity field depends only on the vertical distance z from the electrode surface, the general stationary solutions to

the Navier–Stokes equations in the vapor and film regions are determined apart from four integration constants.

These can be univocally determined by imposing the following boundary conditions on the velocity fields v_f and v_v: (a) $v_v = 0$ very far from the film; (b) $v_v = v_f$ at the film-vapor interface (i.e. no slippage at this boundary); (c) at this interface, the force exerted by the vapor on the film must be equal to that caused by the film on the vapor, that is $\eta_v \left(\frac{dv_v}{dz}\right)_{z=d} = -\eta_f \left(\frac{dv_f}{dz}\right)_{z=d}$; (d) we assume, in general, that there may be slippage at the solid-film interface. Because of this, there will be a frictional force F_{sf} at this boundary. As the last condition, we then impose that the force F_{sf} must be equal and opposite to that due to the film, that is: $F_{sf} = +\eta_f \left(\frac{dv_f}{dz}\right)_{z=0}$. Finally, we make the plausible assumption that F_{sf} depend linearly on the relative velocity between the quartz plate and the film:

$$F_{sf} = -\eta_2 \left[v_0 - v_f(0)\right] \tag{5.6}$$

where η_2 is called coefficient of sliding friction or interfacial viscosity, v_0 is the velocity of the electrode and $v_f(0)$ that of the film at the electrode surface. This condition is consistent with recent QCM studies of the velocity dependence of the interfacial friction [12]. If there is no slippage at the solid-fluid interface, $\eta_2 = \infty$. The opposite limit, $\eta_2 = 0$, corresponds instead to a superfluid whose motion is totally decoupled from that of the oscillating substrate.

By carrying out the necessary algebra, one finds that the reciprocal of Z_{sfv} can be easily rewritten as:

$$\frac{1}{Z_{sfv}} = \frac{1}{Z_v + Z_{fd}} + \frac{1}{\eta_2} \tag{5.7}$$

which says that the total acoustic impedance Z_{sfv} of the combined system substrate-film-vapor can be considered as the parallel between the series of the vapor i mpedance, Z_v, and that of the film Z_{fd}, and the impedance η_2 due to the slippage of the film at the solid boundary.

The formula 5.7 means that it is possible, at least in principle, to measure the friction force of a film adsorbed on a solid surface with a quartz microbalance. In nanotribology one is interested in studying the friction of an adsorbed monolayer. This implies that the acoustic impedance of the film can be simplified as

$$Z_{fd} \simeq -j\,\omega\,\rho_f\,d \tag{5.8}$$

where $\omega = 2\pi f$.

If we solve the 5.7 in terms of R_{sfv} and X_{sfv} we get:

$$\frac{X_{sfv}}{R_{sfv}^2 + X_{sfv}^2} = \frac{\omega\rho_f d + X_v}{R_v^2 + (\omega\rho_f d + X_v)^2} \tag{5.9}$$

and

$$\frac{R_{sfv}}{R_{sfv}^2 + X_{sfv}^2} = \frac{R_v}{R_v^2 + (\omega\rho_f\, d + X_v)^2} + \frac{1}{\eta_2} \tag{5.10}$$

The first equation yields the film thickness d as

$$d = \frac{1}{2\omega\rho_f}\left[R_{sfv}^2 + X_{sfv}^2 + \sqrt{\left(R_{sfv}^2 + X_{sfv}^2\right)^2 - 4R_v^2\, X_{sfv}^2}\right] - \frac{X_v}{\omega\rho_f} \tag{5.11}$$

which can be substituted in the second one in order to calculate the interfacial viscosity η_2.

Finally, the slip time τ_s, which represents the time required for the adsorbed film speed to decay to 1/e of its initial value after that the oscillating substrate has been put to rest in the absence of a bulk vapor, can be calculated from the ratio [3]:

$$\tau_s = \frac{\rho_f\, d}{\eta_2} \tag{5.12}$$

In the limit of very low vapor density, this approach yields identical results with the formulas introduced heuristically by other authors [13], according to which the vapor impedance is in series with the parallel of the film impedance and the interfacial viscosity. As an example, for Kr vapor pressures below 1 Torr, the two approaches yield essentially the same results, while for pressures above 10 Torr this discrepancy can be as high as 15 % or more, depending on the amount of sliding observed.

5.3 QCM Driving Circuits

As we have already mentioned, in order to use the quartz crystal as a nanotribology sensor it is necessary to measure its resonance frequency and its quality factor very accurately. Close to resonance, an AT-plate can in fact be accurately described [10] by the equivalent circuit shown in the enlargement of Fig. 5.1. The capacitor C_0 (of the order of a few pF) represents the static capacitance of the crystal between the two electrodes. The values of L_q and C_q are related to the kinetic and potential energies of the plate. The resistor R_q (of the order of a few tens of Ω) accounts for all the losses of the crystal and thus determines the intrinsic Q_q of the crystal. A quartz plate exhibits a series resonance at $f_s = 1/2\pi\sqrt{L_q C_q}$ and a parallel resonance at f_p where $f_p – f_s \approx f_s C_q / 2C_0$. The detailed values of these characteristic parameters are provided by the manufacturer.

Various techniques have been devised to measure f_{res}. The simplest one is that of the oscillator, which uses the quartz crystal (either at its series or parallel resonance) in a positive feedback network in order to obtain an oscillating circuit. Many different

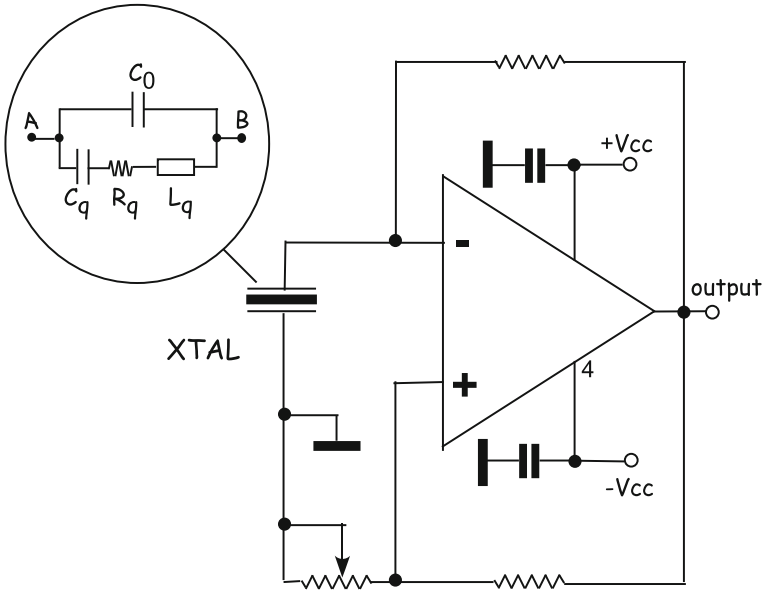

Fig. 5.1 Schematic circuit of a quartz oscillator used in our laboratory

configurations of oscillators exist in the literature. For example, Fig. 5.1 shows a very schematic diagram of an oscillator we have built in which the quartz crystal is connected to the inverting channel of a wide-band operational amplifier. By adjusting the resistance of the trimmer close to R_q, the circuit will auto-oscillate to the series resonance frequency of the quartz.

In practice, because of the unavoidable phase shifts introduced by the electronic components employed, f_{osc} is shifted with respect to f_{res} and this difference depends on the width of the resonance curve, if the overall phase shift does not change. For example, a typical phase error of 10° implies an error in the frequency $\left|\frac{f_{osc}-f_{res}}{f_{res}}\right| \approx 2 \times 10^{-6}$ with a quality factor of 40,000. If Q decreases during the measurements by 30 %, (a value observed in our studies with multilayers and which may become much bigger if one studies systems like heavy, organic fluids characterized by a large damping), it determines a change in the frequency of the oscillator of about 6×10^{-7} parts, e.g. an error of about 3 Hz for a crystal of 5 MHz. Another drawback of the oscillator is that it does not allow an easy variation and monitoring of the excitation power of the crystal. Furthermore, the oscillator selects by itself the resonance mode, typically it is the fundamental series, and it is not easy to switch to other modes. In conclusion, such a technique, although it is the simplest one, is not very flexible and might cause serious measurement errors particularly in situations where the Q of the quartz microbalance is small.

Another simple way to measure both the frequency shift and the dissipation taking place in a QCM experiment is the ring-down QCM, ring-down technique method

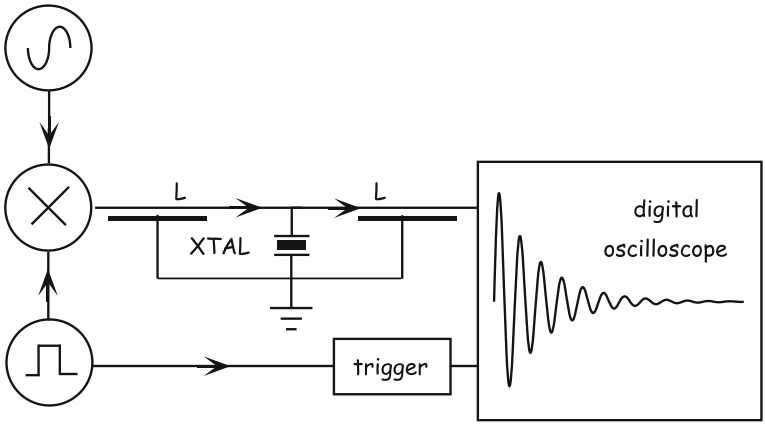

Fig. 5.2 Block diagram of the ring-down technique

shown in Fig. 5.2. The quartz crystal is excited at its resonance frequency either by an high-stability radio frequency generator [14] or by an oscillator [15], which are connected to the electrodes through an electronic switch. This latter one is controlled by a pulse generator that also triggers a digital oscilloscope. In this way, it is possible to turn the excitation on and off at a fixed rate, typically comprised between 10 and 100 Hz, and store the free decaying voltage after the excitation has stopped in the memory of the oscilloscope. The data can then be analyzed and fit according to the function $\mathrm{Aexp}(-\mathrm{t}/\tau)\cos(2\pi\,\mathrm{f}\,\mathrm{t}+\phi)$, where f represents the resonance frequency while the decay time τ is related to the quality factor of the crystal through the simple relation $\mathrm{Q}=\pi\,\mathrm{f}\,\tau$.

In our view, the technique best suited to drive the QCM in nanotribology applications is certainly that of the QCM, frequency modulation technique frequency modulation. In such a technique, $\mathrm{f_{osc}}$ corresponds to the maximum (or to the minimum) of the amplitude of the quartz electrical impedance while the quality factor is deduced from the amplitude of the detected signal [16]. Its main advantages can be summarized as: (i) it is possible to lock on any resonance mode of the QCM (series or parallel, fundamental or overtone) in a very simple and fast way; (ii) the excitation power can be easily varied from a few nW to several μW and, more important for nanotribology studies, its precise value can be accurately determined from the analysis of the crystal circuitry [17]; (iii) it is possible to achieve very high sensitivities and time stabilities; (iv) most of its main components can be easily found in any laboratory.

Figure 5.3 shows the block diagram of the electronics used in the FM technique. The output of an high stability radio-frequency generator equipped with the external frequency-modulation option (FM) drives the quartz crystal (XTAL) with a frequency $\mathrm{f}=\mathrm{f_{car}}+\Delta\mathrm{f}\sin(2\pi\,\mathrm{f_{mod}}\mathrm{t})$, where $\mathrm{f_{car}}$ is the so-called frequency carrier, set by the operator sufficiently close, but not necessarily equal, to the resonance frequency of the quartz mode one wants to lock-on. This $\mathrm{f_{car}}$ is modulated at a low-frequency $\mathrm{f_{mod}}$

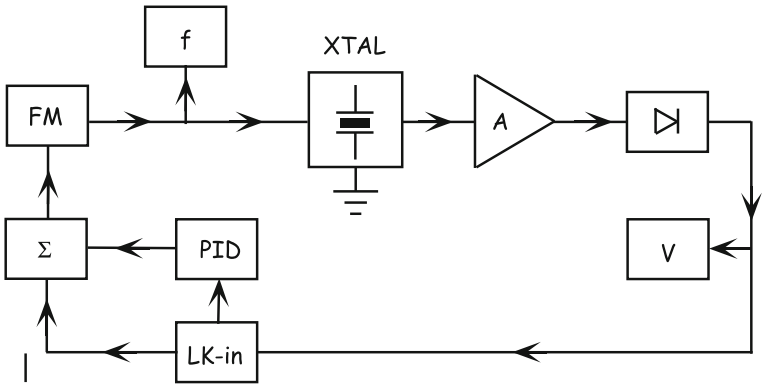

Fig. 5.3 Block diagram of the frequency modulation technique. See text for further details

between the extremes $f_{car} - \Delta f$ and $f_{car} + \Delta f$. The frequency of this modulation has to be smaller than the inverse decay time of the crystal f_{res}/Q_q [16]. The quartz crystal may either be inserted in a transmission line or have one electrode grounded, depending on the experimental set-up. As a matter of course, the actual configuration affects the choice of the amplifier A. If $\Delta f \ll f_{car}$, the amplified voltage can be well approximated by $A(f) \sim A(f_{car}) + \frac{dA(f_{car})}{df} \Delta f \sin(2\pi f_{mod} t)$. The high-frequency component of this signal can then be rectified by a diode detector. In our case, to bypass the problems connected with the use of the diode, e.g. periodic calibrations and thermal and time drifts, we have realized a multiplier whose output yields the square of the signal followed by a low-pass filter [17]. The DC amplitude of this signal is read by a high-precision voltmeter. The small component at f_{mod} is instead detected by a lock-in amplifier (Lk-in). The DC output of Lk-in, which changes sign as the frequency passes through quartz resonance, is used to control the value of f_{car} and thus locks the circuit onto the resonance frequency of the quartz. The block Σ adds up the low frequency modulation signal and the output of the Lk-in. The PID sums up the Lk-in output, its integral and its derivative. The integral is needed to perfectly locate the resonance frequency, the derivative guarantees stability to the feedback loop.

Finally, we mention another simple and sensitive circuit to drive a QCM. A generator is locked to the series resonance of the crystal by an high-frequency lock-in amplifier, which detects the reactive component of the transmission signal of the crystal and shifts the synthesizer frequency to null this component, after an offset is applied to cancel the contributions of shunt capacitance [18].

5.4 Quality of the Surface Electrodes

For a he quantitative use of the QCM in nanotribology, it is of paramount importance to have very homogeneous and well characterized surfaces. In fact, surface roughness not only complicates the comparison with theoretical models but can also prevent

the sliding of the adsorbed film. Although quartz resonators consist of thin disks of single crystalline silicon dioxide which are optically polished on both sides to roughness of about 1 nm rms, the thermally deposited metal electrodes usually exhibit a roughness of a few nm rms. Unfortunately, this roughness cannot be significantly reduced. To anneal a thermally deposited gold electrode, heating above 600 °C would be required. However, at 573 °C a phase transition occurs from α- to β-quartz. This phase transition is reversible upon cooling, but may introduce regions where the direction of the electrical axis in the quartz is reversed and thus remove or greatly reduce the piezoelectricity.

In a systematic study [19] of the surface morphology of Cu films on quartz in a UHV chamber, it was observed that annealing to 340 °C of the films deposited onto quartz preplated with titanium reduces the rms roughness to about 3 nm over a scan size of 500×500 nm^2, although they maintain a self-affine fractal scaling behavior over the length scale $10 \sim 500$ nm.

More recently, Pb films have been grown by physical deposition using an e-beam heated evaporation source at a rate of 0.5 nm/s [20]. The substrate was a quartz blank polished down to an RMS roughness of about 0.3 nm. Prior to Pb evaporation the quartz substrate was annealed under UHV conditions up to 140 °C in order to remove condensed surface impurities. When Pb deposition is performed at or above room temperature, the thermally activated diffusion of Pb atoms is so high that a non connected percolated network of Pb clusters is formed [20]. Therefore, a substrate temperature of 150 K was chosen to hinder adatom mobility and a connected film is formed. In Fig. 5.4 we can see a large scale STM image (2×2 μm) showing the morphology of a 150 nm thick Pb film deposited at 150 K, followed by annealing at

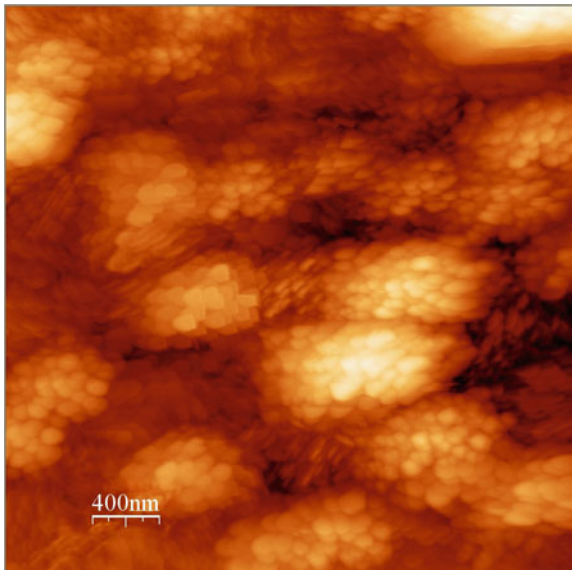

Fig. 5.4 STM topography of a $2{,}000 \times 2{,}000$ nm ^{2} area representative of a 150 nm thick Pb film deposited at 150 K on the surface of an AT-cut quartz. The film is formed by the assembly of 0.5 μm sized domains which are formed by a stacking of platelets. (*Photo* courtesy of F. Buatier de Mongeot)

room temperature. The image shows a distribution of domains with lateral dimensions around 0.5 μm . The various domains can be identified by the different orientation of the platelets. The majority of them are stacked parallel to the quartz surface, with an in-plane rotational mismatch, while a minor fraction is stacked with a tilt angle with respect to the substrate.

Another method to obtain very homogenous surfaces consists in glueing very thin layers of mica to the metal electrodes of a QCM [21]. In this way, it is possible to have a quartz sensor with a macroscopic atomically flat area without a significant loss of its sensitivity. These mica covered crystals have been used in studies of contact mechanics [22]. So far, however, no QCM measurements on the sliding friction of monolayers adsorbed on mica have been reported. Following a similar approach, a piece of Grafoil, a type of graphite, was glued uniformly on the Ag electrodes of a quartz crystal in order to study the slippage of ^{4}He films below 3 K [23].

5.5 UHV Apparatus

Another problem that affects QCM measurements of the sliding friction of adsorbed monolayers is the contamination of the active surface of the quartz sensor [8]. To overcome these problems, we have recently assembled a new apparatus specifically designed to perform friction experiments on molecularly thin films carried out with the QCM technique in ultra-high-vacuum and at a temperature as low as 4 K [24]. The main chamber is provided with a stainless steel jacket that allows a quick change of the various temperature inserts (cryocooler head, liquid nitrogen insert, Peltier-cell stage…) that span the working range 4–400 K, without ever breaking the vacuum. The crystal mounting is compatible with UHV conditions and with the Omicron standard and guarantees a good thermal and electrical contact over the entire temperature range. The quartz is inserted in a specially designed copper sample holder, housing the wiring for the temperature control and signal detection systems in a volume separated by that of the chamber. In this way, we can control the QCM temperature within 5 mK or less at any temperature below 10 K. Furthermore, the quartz frequency and amplitude stabilities are found to be as good as the best recorded values achieved with QCMs mounted in standard high-vacuum, liquid bath cryostats. The system is provided with a sputtering ion gun mounted in the fast-entry load section to clean the QCM electrodes from surface contaminants. The movements of the quartz sample inside the vacuum volume of the system are performed through the combination of a magnetic translator and a wobble stick.

Facing the circular hole in the crystal mounting, there is a thin-wall stainless steel tube whose end is attached to a sapphire variable leak valve. The high pressure side of the valve is connected to a high-purity gas cylinder and another port allows to purge the system effectively. A film is condensed onto the QCM, kept at low temperature, by slowly leaking gas through this nozzle. Depending onto the vapor pressure, the film may cover either only one or both electrodes. In the former case, which typically occurs at very low temperatures, the deposition of a Ne film can be controlled within

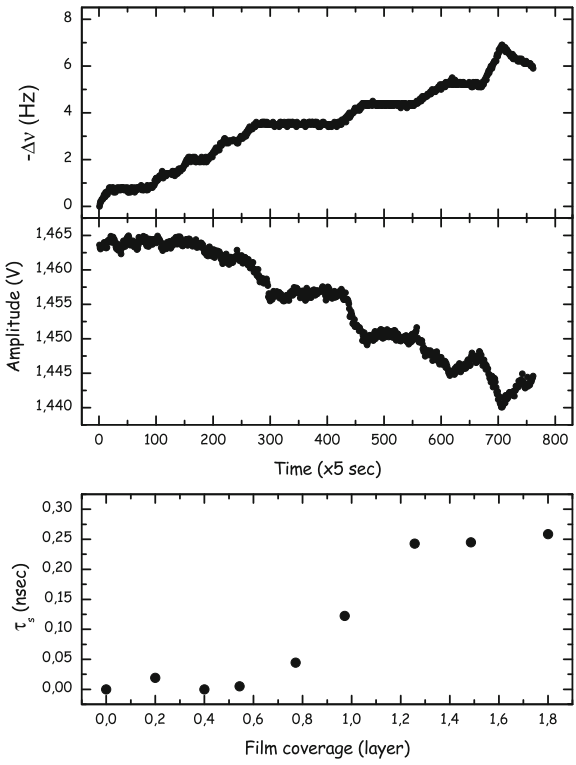

Fig. 5.5 Raw data of the resonance frequency shift (*top*) and amplitude (*middle*) during an adsorption isotherm of Ne on lead at 6.5 K. *Bottom* calculated slip time as a function of Ne film coverage

0.1 layers working at a fundamental frequency of 5 MHz. Obviously, this figure improves significantly using an heavier adsorbate and/or an higher overtone. For instance, the dosing of a Kr film onto a QCM running at 15 MHz (and third overtone) is done with a resolution better than 0.05 layers. If necessary, the adsobed film can be annealed to higher temperatures by simply turning off the cryocooler.

In the following, we present some preliminary data acquired with this setup at temperatures below 10 K. They refer to Ne deposited on a Pb(111) electrode grown and characterized in the group of Prof. Valbusa following the procedure described in the previous section. The data have been acquired at the third overtone of a 5 MHz quartz plate characterized by a quality factor of 380,000 at low temperatures. The two top graphs in Fig. 5.5 show the variations in the measured QCM resonance parameters during Ne evaporation. By acting on the leak valve, the film was slowly grown in steps of about 0.2 layers and then we waited for the system to equilibrate. At low coverages, there is no change in the quartz amplitude and accordingly the slip time is zero. Close to 0.4–0.5 layers, dissipation starts to appear and the slip time reaches values close to 0.3 ns, which are typical for rare gases sliding on metal surfaces. The slip times described in the bottom of Fig. 5.5 have been normalized with coverage according to the formulas reported in [8].

Although there is no data available in the literature on the 2D phase diagram of Ne adsorbed on Pb(111), it is tempting to interpret our data in terms of a structural depinning of the film. At low coverages, the Ne film is in a fluid phase that at such low temperatures is locked to the substrate. Close to about 0.4 layers, the film enters an incommensurate solid phase which is weakly bound to the substrate and can easily slides. This interpretation is consistent with the structural phase diagrams of heavy rare gases adsorbed on Ag(111) [25], systems that are very similar to Ne/Pb(111). Our measurements are also in very good qualitative agreement with the results of extensive computer simulations of a model system carried out by Persson [26] in the case of a low-corrugated substrate.

A systematic study of the dependence of the slip time on film coverage, driving amplitude and temperature is currently under way in order to establish the phase diagram of this intrinsic depinning [27]. In a previous QCM study of the sliding friction of Kr monolayers adsorbed on Au(111) at 85 K we have also observed a nonlinear behavior, but in that case the depinning was induced by increasing the driving amplitude above a certain threshold [7]. More recently, highly sensitive AFM experiments have found changes in the friction behavior that are based on similar structural effects. Dienwiebel et al. observed that friction between graphite surfaces is significantly reduced when the surfaces are rotated out of the commensurate locking angle [28]. Socoliuc et al. by varying the normal load on the contact between tip and substrate, have also observed a new regime of very low friction in which negative and positive lateral forces sum up to a vanishing average force in the time average instead of the spatial average [29].

It is a pleasure to acknowledge several clarifying explanations of the theoretical aspects of nanofriction we have had over the past few years with Francesco Ancilotto, Bo Persson and Erio Tosatti. We also wish to thank our experimental partners Francesco Buatier de Mongeot, Renato Buzio, Bruno Torre, Corrado Boragno and Ugo Valbusa for many interesting discussions and suggestions. We have greatly benefitted from daily interactions with our students who have been involved with these studies: Alessandro Carlin, Moira Ferrari, Luca Stringher, Francesco dalla Longa, Giovanni Fois and Alberto Pontarollo, and we must also thank Giorgio Delfitto for his technical mastery. Finally, funding from INFM, PRA *Nanorub*, and MIUR, FIRB *Carbon based micro and nanostructures* and PRIN *Nanotribologia,* is kindly acknowledged.

References

1. B.N.J. Persson, *Sliding Friction* (Springer, Berlin, 1998), Chap. 1
2. J. Krim, Sci. Am. **275**, 74 (1996)
3. J. Krim, A. Widom, Phys. Rev. B **38**, 12184 (1988)
4. J. Krim, D.H. Solina, R. Chiarello, Phys. Rev. Lett. **66**, 181 (1991)
5. C. Daly, J. Krim, Phys. Rev. Lett. **76**, 803 (1996)
6. R.L. Renner, P. Taborek, J.E. Rutledge, Phys. Rev. B **63**, 233405 (2001)
7. L. Bruschi, A. Carlin, G. Mistura, Phys. Rev. Lett. **88**, 046105 (2002)

8. A. Carlin, L. Bruschi, G. Mistura, Phys. Rev. B **68**, 045420 (2003)
9. G. Hayderer, M. Schmid, P. Varga, H.P. Winter, F. Aumayr, Rev. Sci. Instrum. **70**, 3696 (1999)
10. J.C. Brice, Rev. Mod. Phys. **57**, 105 (1985)
11. L. Bruschi, G. Mistura, Phys. Rev. B **63**, 235411 (2001)
12. C. Mak, J. Krim, Phys. Rev. B **58**, 5157 (1998)
13. E.T. Watts, J. Krim, A. Widom, Phys. Rev. B **41**, 3466 (1990)
14. S. Berg, T. Prellberg, D. Johannsmann, Rev. Sci. Instrum. **74**, 118 (2003)
15. M. Rodahl, F. Höök, A. Krozer, P. Brzezinski, B. Kasemo, Rev. Sci. Instrum. **66**, 3924 (1995)
16. M.J. Lea, P. Fozooni, P.W. Retz, J. Low Temp. Phys. **54**, 303 (1984)
17. L. Bruschi, G. Delfitto, G. Mistura, Rev. Sci. Instrum. **70**, 153 (1999)
18. G.B. Hess, M.J. Sabatini, M.H.W. Chan, Phys. Rev. Lett. **78**, 1739 (1997)
19. S.M. Lee, J. Krim, Thin Solid Films **489**, 325 (2005)
20. B. Torre, F. Buatier de Mongeot, F. Krok, R. Alessio, C. Boragno, U. Valbusa, to be published
21. S. Berg, M. Ruths, D. Johannsmann, Rev. Sci. Instrum. **74**, 3845 (2003)
22. S. Berg, D. Johannsmann, Phys. Rev. Lett. **91**, 145505 (2003)
23. N. Hosomi, A. Tanabe, M. Hieda, M. Suzuki, J. Low Temp. Phys. **138**, 361 (2005)
24. L. Bruschi, A. Carlin, F. Buatier de Mongeot, F. dalla Longa, L. Stringher, G. Mistura, Rev. Sci. Instrum. **76**, 023904 (2005)
25. J. Unguris, L.W. Bruch, M.B. Webb, J.M. Phillips, Surf. Sci. **114**, 219 (1982)
26. B. Persson, Phys. Rev. B **48**, 18140 (1993)
27. L. Bruschi et al., to be published
28. M. Dienwiebel, G. Verhoeven, N. Pradeep, J. Frenken, J. Heimberg, H. Zandbergen, Phys. Rev. Lett. **92**, 126101 (2004)
29. A. Socoliuc, R. Bennewitz, E. Gnecco, E. Meyer, Phys. Rev. Lett. **92**, 134301 (2004)